Cancer Letters 460 (2019) 108–118

Contents lists available at ScienceDirect

Cancer Letters

journal homepage: www.elsevier.com/locate/canlet

Original Articles

A recombinant measles virus vaccine strain rMV-Hu191 has oncolytic effect against human gastric cancer by inducing apoptotic cell death requiring integrity of lipid raft microdomains

Yao Lv[a], Duo Zhou[a], Xiao-qiang Hao[a], Meng-ying Zhu[a], Chu-di Zhang[a], Dong-ming Zhou[b], Jin-hu Wang[b], Rong-xian Liu[a], Yi-long Wang[b], Wei-zhong Gu[b,c], Hong-qiang Shen[b,c], Xi Chen[a,b,c,*], Zheng-yan Zhao[a,b,c,**]

[a] Zhejiang University School of Medicine, Hangzhou, 310000, Zhejiang, China
[b] Children's Hospital, Zhejiang University School of Medicine, Hangzhou, 310052, Zhejiang, China
[c] Key Laboratory of Diagnosis and Treatment of Neonatal Diseases of Zhejiang Province, Hangzhou, 310052, Zhejiang, China

ARTICLE INFO

Keywords:
Gastric cancer
rMV-Hu191
Oncolytic virotherapy
Apoptosis
Lipid rafts

ABSTRACT

Live-attenuated strain of measles virus (MV) has oncolytic effect. In this study, the antitumor effect of rMV-Hu191, a recombinant Chinese Hu191 MV generated in our laboratory by efficient reverse genetics system, was evaluated in gastric cancer (GC). From our data, rMV-Hu191 induced cytopathic effects and inhibited tumor proliferation both in vitro and in vivo by inducing caspase-dependent apoptosis. In mice bearing GC xenografts, tumor size was reduced and survival was prolonged significantly after intratumoral injections of rMV-Hu191. Furthermore, lipid rafts, a type of membrane microdomain with specific lipid compositions, played an important role in facilitating entry of rMV-Hu191. Integrity of lipid rafts was required for successful viral infection as well as subsequent cell apoptosis, but was not required for viral binding and replication. CD46, a MV membrane receptor, was found to be partially localized in lipid rafts microdomains. This is the first study to demonstrate that Chinese Hu191 MV vaccine strain could be used as a potentially effective therapeutic agent in GC treatment. As part of the underlying cellular mechanism, the integrity of lipid rafts is required for viral entry and to exercise the oncolytic effect.

1. Introduction

Oncolytic virotherapy is a cancer therapeutic platform established and extensively studied in the past two decades. In 2005, Oncorine was approved by SFDA in China as the first oncolytic virus medicine in the world to treat nasopharyngeal carcinoma [1]. Later, other strains have been approved in the US and Europe and registered in anticancer treatment [2,3]. The advantageous property of oncolytic viruses is their selective replication in tumor cells over the normal cells, especially the genetically modified strains. Measles virus (MV) is one of the oncolytic viruses, and its antitumor efficiency has been evaluated and demonstrated in more than twelve different cancer types [4]. Phase I/II clinical trials using Edmonston strain MV are currently underway, recruiting patients with relapsed or recurrent cancers including breast cancer, ovarian cancer, multiple myeloma, mesothelioma, and glioma [5,6].

MV is a negative strand RNA paramyxovirus [7]. Its genome encodes six structural proteins, the fusion protein MV-F, the haemagglutinin MV-H, a phosphoprotein MV-P, the nucleoprotein MV-N, the matrix protein MV-M, and an RNA polymerase MV-L. Two non-structural proteins, MV-V and MV-C, are not present within the virion [8]. The Chinese measles vaccines are widely used in China for more than 50 years, and have an outstanding safety record [9]. The oncolytic effect of the rMV-Hu191 vaccine strain against lung carcinoma has been reported [10]. Recently in our laboratory, an efficient reverse genetics system has been successfully established [11], and will allow further

* Corresponding author. Children's Hospital, Zhejiang University School of Medicine, 3333 Bin Sheng Rd, Bin Jiang District, Hangzhou, Zhejiang, 310052, China.
** Corresponding author. Children's Hospital, Zhejiang University School of Medicine, 3333 Bin Sheng Rd, Bin Jiang District, Hangzhou, Zhejiang, 310052, China.
E-mail addresses: 21418068@zju.edu.cn (Y. Lv), 11318120@zju.edu.cn (D. Zhou), 11718196@zju.edu.cn (X.-q. Hao), 11618182@zju.edu.cn (M.-y. Zhu), 21718442@zju.edu.cn (C.-d. Zhang), 21318243@zju.edu.cn (D.-m. Zhou), wjh@zju.edu.cn (J.-h. Wang), 21618412@zju.edu.cn (R.-x. Liu), 11418155@zju.edu.cn (Y.-l. Wang), 6195013@zju.edu.cn (W.-z. Gu), shenhq@zju.edu.cn (H.-q. Shen), chchenxi@zju.edu.cn (X. Chen), zhaozy@zju.edu.cn (Z.-y. Zhao).

https://doi.org/10.1016/j.canlet.2019.06.010
Received 5 January 2019; Received in revised form 5 June 2019; Accepted 13 June 2019

modification of the virus for enhanced selectivity and higher antitumor potency. This MV vaccine strain may serve as a promising candidate for oncolytic virotherapy.

Gastric cancer (GC) is the fifth most common malignancy worldwide, and the overall mortality rate of GC is the third highest of all types of cancers [12]. Although conventional treatment procedures including surgery and chemotherapy have made significant improvements in survival of GC patients, less than 25% of cases are actually eligible for surgery [13]. In patients undergoing chemotherapy, drug resistance and tumor recurrence frequently occurs [14,15]. With the 5-year survival rate as low as 30.6%, GC remains a threatening type of cancer [13]. Thus, efforts to develop new, efficient drugs for the treatment of GC are constantly ongoing. Many different classes of viruses with natural or modified specificity have been explored as therapeutics for GC, such as herpes simplex virus (HSV) type 1, adenovirus echovirus 1, Newcastle disease virus, reovirus, and vaccinia virus [16–20]. However, whether or not the live-attenuated MV strain Chinese Hu-191 strain can target GC remains unknown. To mediate viral entry, there are three identified host-cell receptors of MV vaccine strains, nectin-4, signaling lymphocyte-activation molecule (SLAM) or CD150, and CD46 [21]. Both CD46 and nectin-4 was expressed in human GC cells [22,23]. This study evaluated the potential antitumor activity of the generated rMV-Hu191 against human GC cell lines and xenografts and investigated the underlying mechanism that facilitates viral entry.

Cell membranes are not heterogeneous but are dynamically organized in microdomains. Cholesterol and sphingolipid-rich membrane domains termed as 'lipid rafts' were identified from biomembranes several decades ago, and have been shown to play functional roles in protein endocytosis and signaling pathways [24,25]. Lipid rafts are involved in both viral entry [26,27] and exocytosis [28] in host cells. Interestingly, in lipid rafts, both CD46 [29] and structural proteins of MV [30,31] have been found. In the literature, there is lack of evidence showing that lipid raft integrity is required for MV viral binding or entry; however, the intracellular assembly of MV might require lipid rafts [32]. In GC, lipid rafts were proved to mediate caspase-dependent apoptosis [33,34]. Thus we hypothesize that rMV-Hu191 may require lipid rafts to exhibits its oncolytic effects.

2. Materials and methods

2.1. Cell lines and culture

African green monkey kidney Vero cells purchased from the American Type Culture Collection (ATCC, USA) were cultured in Dulbecco's modified Eagle's medium (DMEM, Life Technologies, USA) supplemented with 10% fetal bovine serum (FBS, Life Technologies, USA). The BGC-823 and SGC-7901 cells were both purchased from the Cell Bank of the Chinese Academy of Sciences, Shanghai, China, and maintained in RPMI 1640 medium (Life Technologies, USA) supplemented with 10% FBS and 100 U/ml penicillin-streptomycin (Life Technologies, USA). All cells were cultured in a humidified atmosphere of 5% CO_2 at 37 °C.

2.2. Virus strain, titration and infection assays

The construction of recombinant MV (rMV-Hu191) was carried out by efficient reverse genetics system in our laboratory. The sequence of rMV-Hu191 is identical with the published Hu191 sequence (GenBank accession No. FJ416067). Propagation and purification of rMV-Hu191 was previously described [11]. The tissue culture infective dose (TCID 50) was determined by 50% end point dilution assays on Vero cells according to the Reed and Muench method [35] to calculate the titers of viral stocks and other virus-containing samples. For virus infection assays, 2×10^5 cells were seeded on 6-well culture plates (Corning, USA) and cultured for 24 h, then incubated with rMV-Hu191 at a certain multiplicity of infection (MOI) in Opti-MEM medium (Life Technologies, USA) for 2 h at 37 °C. At the end of the incubation period, medium containing virus was removed, the cells were washed by phosphate buffered saline (PBS, Jinuo, China), and then fresh maintenance media was added. The cells were then subjected to viability assays etc as described below. To determine the amount of virus unbound to cells, after 2 h' incubation with virus to allow sufficient time for binding, the virus-containing medium was collected and titration was determined by TCID 50. To determine the titer of total virus, cells and supernatant were collected. Samples were subjected to two cycles of freezing and thawing between −80 °C and 37 °C, centrifuged at 3600 × g (Allegra 6R, Beckman Coulter, USA) for 15 min and stored at −80 °C. The supernatant was used to titrate for measles virus by TCID 50 assay on Vero cells as described above.

2.3. Cell viability assay

BGC-823 Cells and SGC-7901 cells were plated at 4×10^3 cells or 3×10^3 cells per well in 96-well plates cultured for 24 h before incubation with rMV-Hu191 at different MOI for different time periods. To induce or to inhibit caspase-dependent apoptosis, staurosporine (STS) and Z-VAD (both from Apexbio Technology, USA) were administered respectively. The maintenance media were then removed and the cells were then incubated with 10 μl of commercially available CCK-8 reagent (Dojindo Molecular Technologies, Japan) and 100 μl RPMI 1640 medium for 1 h at 37 °C. The relative absorbance at OD 450 nm was measured, and cell viability was calculated based on standard curves.

2.4. Flow cytometry analysis

After the desired treatments, BGC-823 and SGC-7901 cells were collected, fixed and stained as instructed by an apoptosis detection kit (BD Biosciences, USA). Briefly, cells were trypsinized, washed by PBS, and resuspended at the density of 1×10^6 cells/ml in 1 × binding buffer, then incubated with Annexin V-fluorescein isothiocyanate (FITC) and propidium iodide (PI) reagents. Cells were analyzed on a flow cytometer (Navios, Beckman Coulter, USA), and the data were processed by Flowjo 10.0 software (Tree Star Inc, USA).

2.5. Evaluation of cytopathic effects (CPEs) in vitro

The BGC-823 and SGC-7901 cells were cultured in 24-well plates at a density of 2×10^5 or 1×10^5 cells per well. The cells were infected with rMV-Hu191 at a MOI of 0.1 or 1 for 2 h. The virus suspension was then removed, and 1 ml of fresh medium was added to each well. After 48, 72 or 96 h of viral infection, the cells were gently washed with PBS and the remaining cells were fixed in 4% (v/v) paraformaldehyde (PFA) in PBS for 2 h, and stained with 0.05% (w/v) crystal violet (Solarbio, China). Remaining attached cells were photographed under light microscope (Zeiss, Germany) with companion software.

2.6. Immunofluorescence (IF)

Lipid rafts microdomains were visualized by cholera toxin subunit B (CTB) that binds to ganglioside GM1, a "raft"-specific lipid species [36]. For colocalization analysis, BGC-823 and SGC-7901 cells after desired treatment were incubated with Alexa 488-conjugated CTB (C-34775, Invitrogen, USA) for 120 min at 37 °C in fresh maintenance media, followed by fixation by 4% PFA for 30 min on ice, permeation by 0.1% TritonX-100, blocking by 2% BSA, then incubated with anti-measles virus phosphoprotein (MV-P, ab43820, Abcam, UK), or with anti-CD46 (AA2102 N, Thermofisher, USA) at 4 °C overnight, followed by Alexa Fluor® 594 conjugated secondary antibodies (#1596064 and #1608644, Life Technologies, USA), and then with DAPI (Beyotime, China) in the dark. Unspecific bindings have been excluded in other

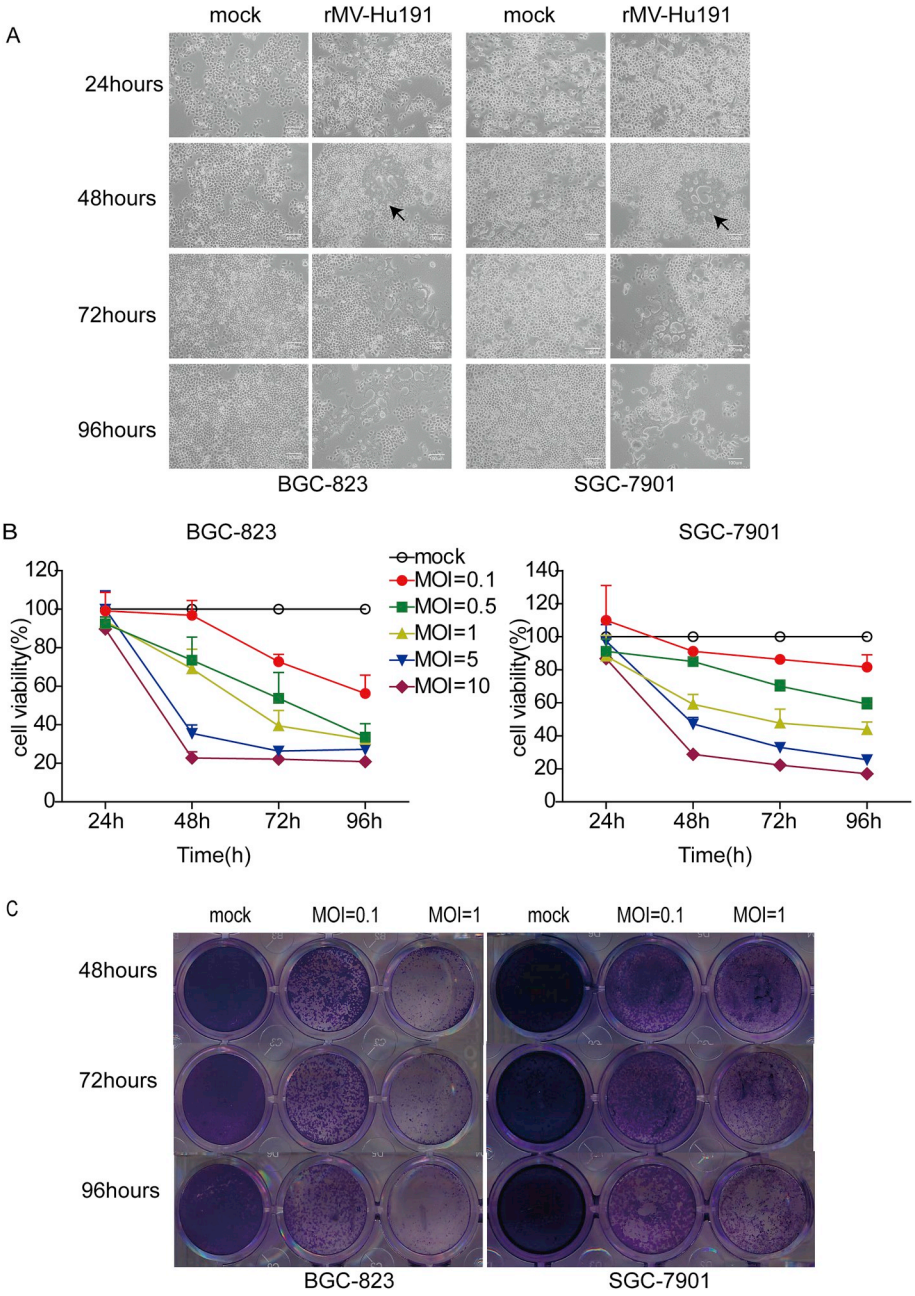

Fig. 1. The infectivity and oncolytic effect of rMV-Hu191 in human GC cells. (A) Morphological changes of BGC-823 and SGC-7901 cells after viral infection at different time points. Scale bar = 100 μm. Arrows indicate syncytia induced by rMV-Hu191. (B) Viability of BGC-823 and SGC-7901 cells after viral infection with different MOIs at different time points. Data were presented as mean ± SE from three repeated experiments with five parallel repeats in each experiment. (C) Analysis of virus-induced CPE by crystal violet staining. (For interpretation of the references to color in this figure legend, the reader is referred to the Web version of this article.)

samples using primary or secondary antibodies only. Slides were photographed using an Olympus BX61WI-FV1200MPE confocal laser scanning microscope and companion software. For IF imagining of MV-P only, cells were fixed, permeated, blocked and incubated with anti-MV-P (ab43820, Abcam, UK) and secondary antibody, then photographed by Zeiss cLSM780 confocal laser scanning microscope and companion software.

2.7. Disruption and solubilization of cholesterol-rich 'lipid rafts'

The cholesterol-rich lipid rafts allows solubilization by non-ionic detergents such as Triton X-100 [37] and extraction from biomembranes by methyl-β-cyclodextrin (MβCD) [38], allowing its functional roles to be investigated in cultured cells. To disrupt lipid rafts in cultured cells, cells were incubated with culture medium containing 5 mM MβCD at 37 °C for 2 h before maintenance in fresh medium.

To obtain 'lipid rafts' membrane fractions, BGC-823 and SGC-7901 cells after desired treatments were resuspended in ice-cold solubilization buffer supplemented with protease inhibitors, and solubilized by non-ionic detergent TritonX-100 as previously described [39]. Cells were homogenized by passing through 26G needle with syringe for 30 times. Nuclei were pelleted at 500 ×g at 4 °C for 5 min (Allegra 6R, Beckman Coulter, USA). The supernatant was collected and the protein concentration was determined by commercial assay kit (Beyotime, China). The membrane preparations were adjusted with solubilization buffer to a final protein concentration of 5 mg/ml, and mixed with equal volume of TritonX-100 (Solarbio, China) with the concentration of 0.5% (w/v, in solubilization buffer). Solubilization was carried out at 4 °C for 20 min. Solubilized membrane fractions were diluted 1:1 with 80% sucrose and loaded at the bottom of the centrifuge tubes. Density gradients made of 5–35% sucrose were layered on top, then centrifuged with a swing bucket rotor at 200,000 ×g for 14 h at 4 °C (Optima ultracentrifuge, Beckman Coulter, USA). Afterwards, 10 serial aliquots with equal volume were collected from the top to the bottom of the sucrose gradient, labelled as 1 to 10, and each was mixed with 5 × loading buffer. Pellets were resuspended in equal volume of

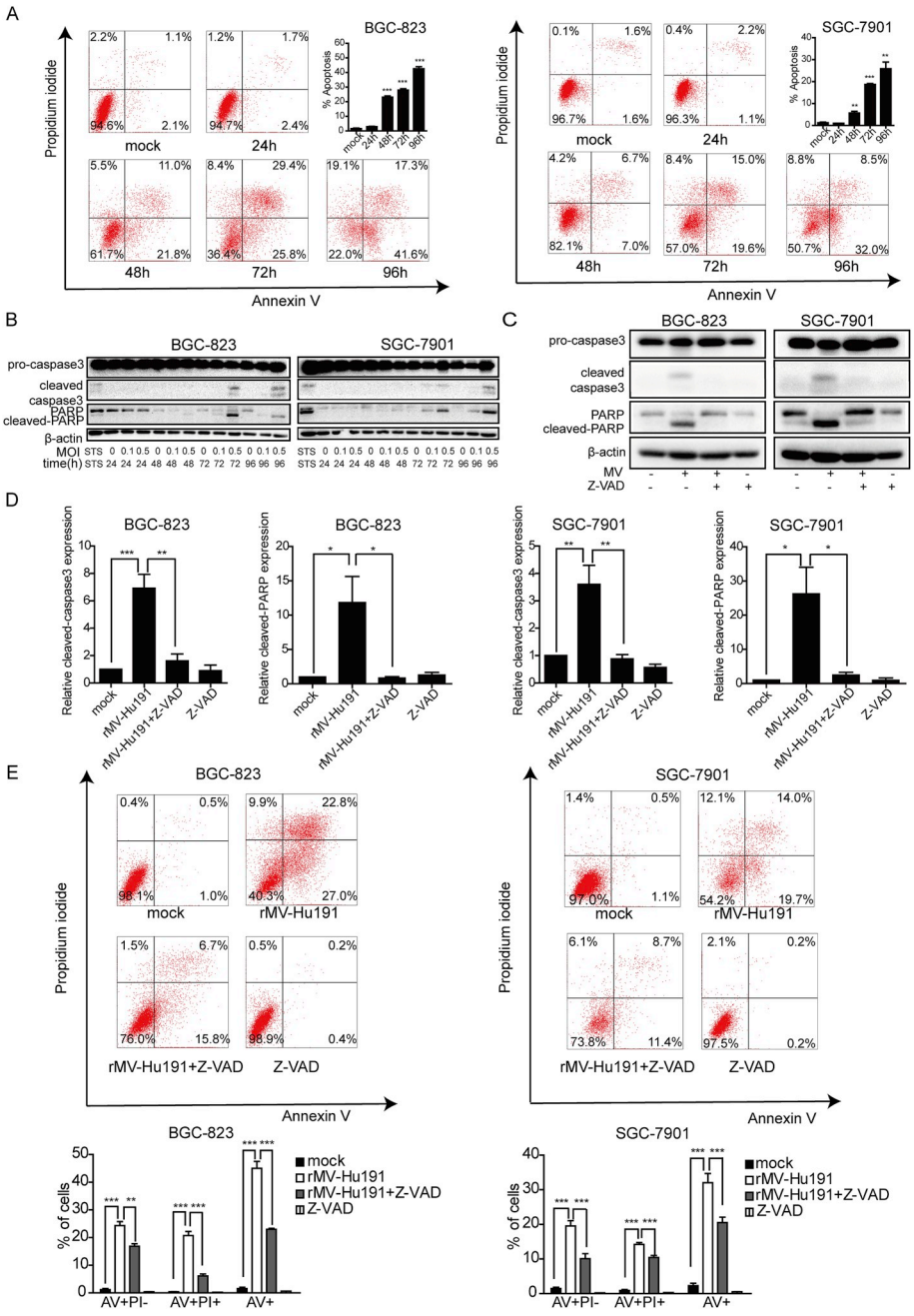

Fig. 2. rMV-Hu191 promoted caspase-dependent apoptosis in human GC cells. (A) Ratio of apoptotic cells after rMV-Hu191 infection in BGC-823 and SGC-7901 cells by flow cytometry analysis. (B) Expression of cell apoptosis markers pro-caspase 3, cleaved caspase 3, PARP, and cleaved PARP in BGC-823 and SGC-7901 cells after rMV-Hu191 infection at different time points. Staurosporin (STS, 500 nM for 24 h) was used to induce caspase-dependent apoptosis. (C) Expression cell apoptosis markers after co-treatment of pan-caspase inhibitor Z-VAD (50 μM for 72 h). (D) Densitometry analysis of the expression of cleaved caspase 3 and cleaved PARP using β-actin as the internal control. (E) Ratio of apoptotic cells after co-treatment of Z-VAD and rMV-Hu191. *:P < 0.05, **:P < 0.01, ***: P < 0.001.

1 × loading buffer. All fractions underwent Western blotting as described below, and lipid rafts fractions were identified by enrichment of a marker protein flotillin 1 [40].

2.8. Western blotting

After desired treatments, cells were lysed in RIPA buffer (Beyotime, China) supplemented with protease and phosphatase inhibitors for 15 min on ice. The pellet was discarded after centrifugation and the protein concentration from the supernatant was determined by commercial kit. A total of 30 μg of protein was loaded onto each well of the SDS-PAGE gel. Page Ruler Prestained Protein Ladder (Thermo Fisher Scientific, USA) was loaded in a separate well together with the samples onto the gel and underwent electrophoresis, followed by transferring onto Immuno-Blot PVDF membrane (Bio-Rad Laboratories, USA). The membranes were blocked in defat milk at room temperature (RT) for 1 h, then incubated with primary antibodies at 4 °C overnight, followed by secondary antibodies at RT for 1 h. The bands were detected using enhanced chemiluminescence detection kit (Biological Industries, Israel). The following primary antibodies were used: anti-MV-P (ab43820, Abcam, UK), anti-CD46 (ab108307, Abcam, UK), anti-nectin-4 (AF2659, R&DSystems, USA), anti–flotillin 1 (ab133497, Abcam, UK), and anti-β-actin (#4970S), anti-caspase-3 (#9665S), anti-PARP (#9542S) antibodies (all from Cell Signaling Technology, USA). Secondary antibodies include HRP-conjugated anti-rabbit IgG (#7074S) and anti-mouse IgG (#7076S) (both from Cell Signaling Technology, USA), and anti-goat IgG (# RAG007, Multi Sciences, China). Each experimental condition was repeated for at least 3 times and representative blots were presented. ImageJ 1.45S software (National Institutes of Health, USA) was used to analyze the densitometry of the blots.

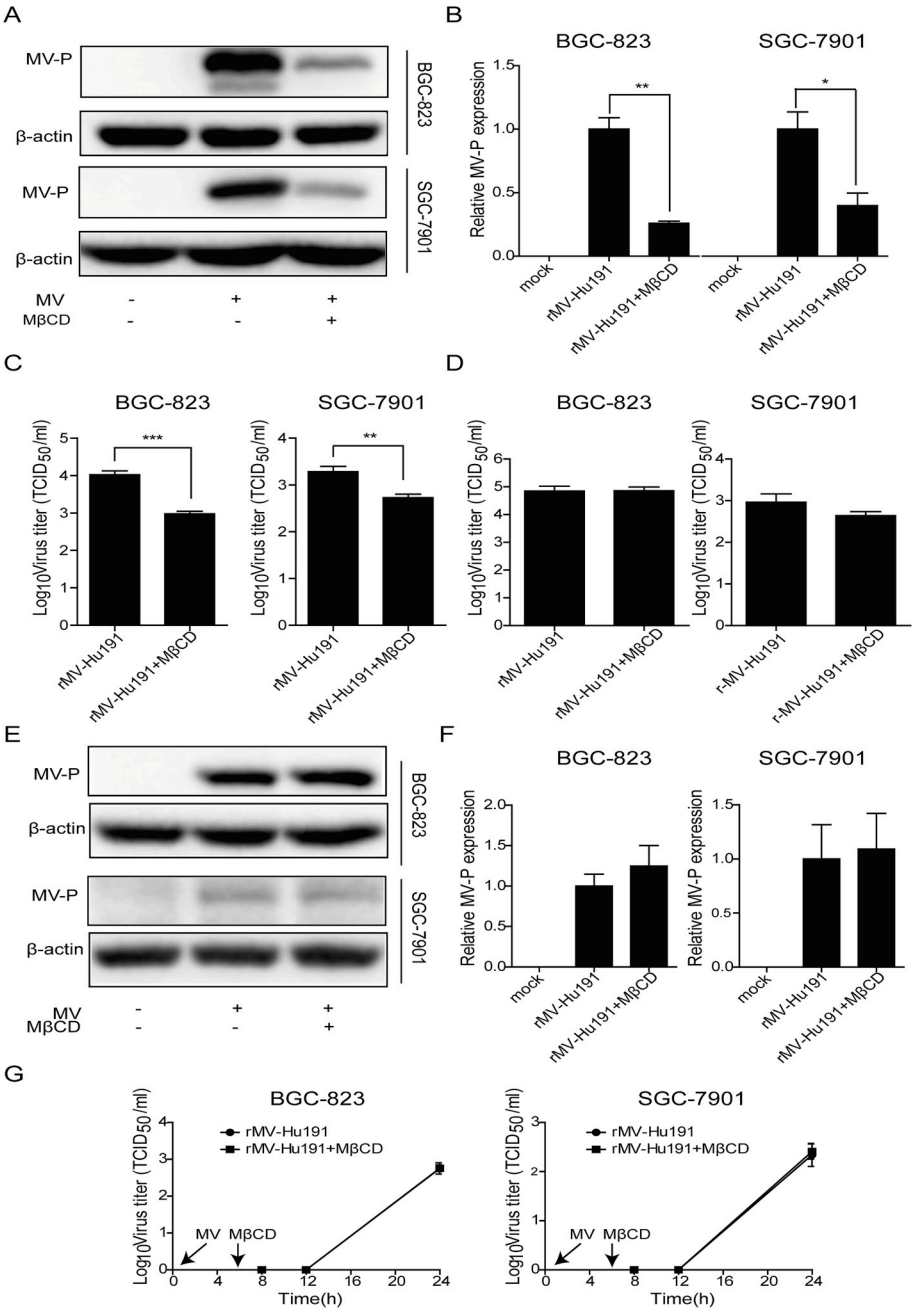

Fig. 3. Lipid raft integrity was required for rMV-Hu191 viral particle entry, but not for binding or replication. (A) MV-P levels in GC cells 24 h after rMV-Hu191 infection (MOI = 1), with or without MβCD treatment (5 mM, 2 h) prior to infection. (B) The densitometry analysis using β-actin was used as internal control. (C) TCID50 of rMV-Hu191 collected from GC cells after 24 h' infection (MOI = 1) with or without MβCD treatment (5 mM, 2 h) prior to viral infection. (D) TCID 50 from the virus-containing medium after cells were incubated with rMV-Hu191 for 2 h to allow binding, with or without MβCD pretreatment. MOI was 4 and 1 in BGC-823 and SGC-7901 cells, respectively. (E–F) BGC-823 and SGC-7901 cells were treated with MβCD for 2 h prior to rMV-Hu191 infection (MOI = 1) for 2 h. Expression of MV-P protein from the cell lysates (E) and the quantitative densitometry analysis from repeated blots (F). (G) GC cells were infected by virus-containing medium for 2 h, and MβCD was added at 6 h after infection. Viral titer was determined at 8, 12 and 24 h after infection. **:P < 0.01, ***:P < 0.001.

2.9. In vivo GC tumor model

The animal experiments were approved by the animal ethical committee of Zhejiang University. Male nude mice aged 3–5 weeks were purchased and housed under standard conditions in the animal center of Zhejiang Chinese Medical University, Hangzhou, Zhejiang, China. GC tumor models were established in mice by subcutaneous injection of SGC-7901 cell suspensions at 2×10^6 cells in 100 μl PBS in the right flank.

The tumor dimensions were recorded by vernier caliper, and the volume was calculated as $V = 0.5 \times (\text{length} \times \text{width}^2)$. On post-implantation day 7, the average volume reached 50–100 mm^3, mice were randomly divided into two groups, 10 in each group. From this day, mice from the rMV-Hu191 treatment group received intratumoral injections of 1.4×10^7 (TCID 50) of virus suspension in 100 μl Opti-MEM 6 times on post-implantation days 7, 8, 9, 11, 13 and 15, while the mice from the mock treated group were injected with equal volume of Opti-MEM. On post-implantation day 15, 3 mice from each group were sacrificed to collect tumor tissues for detection of in situ apoptosis and virus replication. Proteins were also extracted from fresh tissues and subjected to Western blotting. The other 7 mice from each group were housed till day of death or euthanasia. Tumor volumes and weight were monitored every third day on the first 16 days after tumor implantation, and daily after day 16, and tumor-bearing mice were euthanized when over 20% body weight loss occurred, or when tumor diameter exceeded 15 mm.

Tumor tissues were fixed in 4% PFA, embedded in paraffin, sectioned into 4 μm slices (HM-340E, Microm, Germany), and stained by hematoxylineosin (HE). For immunohistochemistry analysis, sectioned paraffin-embedded tumor tissues were stained using anti-cleaved caspase 3 antibody (#9664, Cell Signaling Technology, USA) for 60 min at 37 °C. After being rinsed in PBS twice, the slides were incubated with HRP polymer at 37 °C for 30 min, followed by counterstaining with hematoxylin for 1 min, rinsing in tap water for 1 min. The slides were

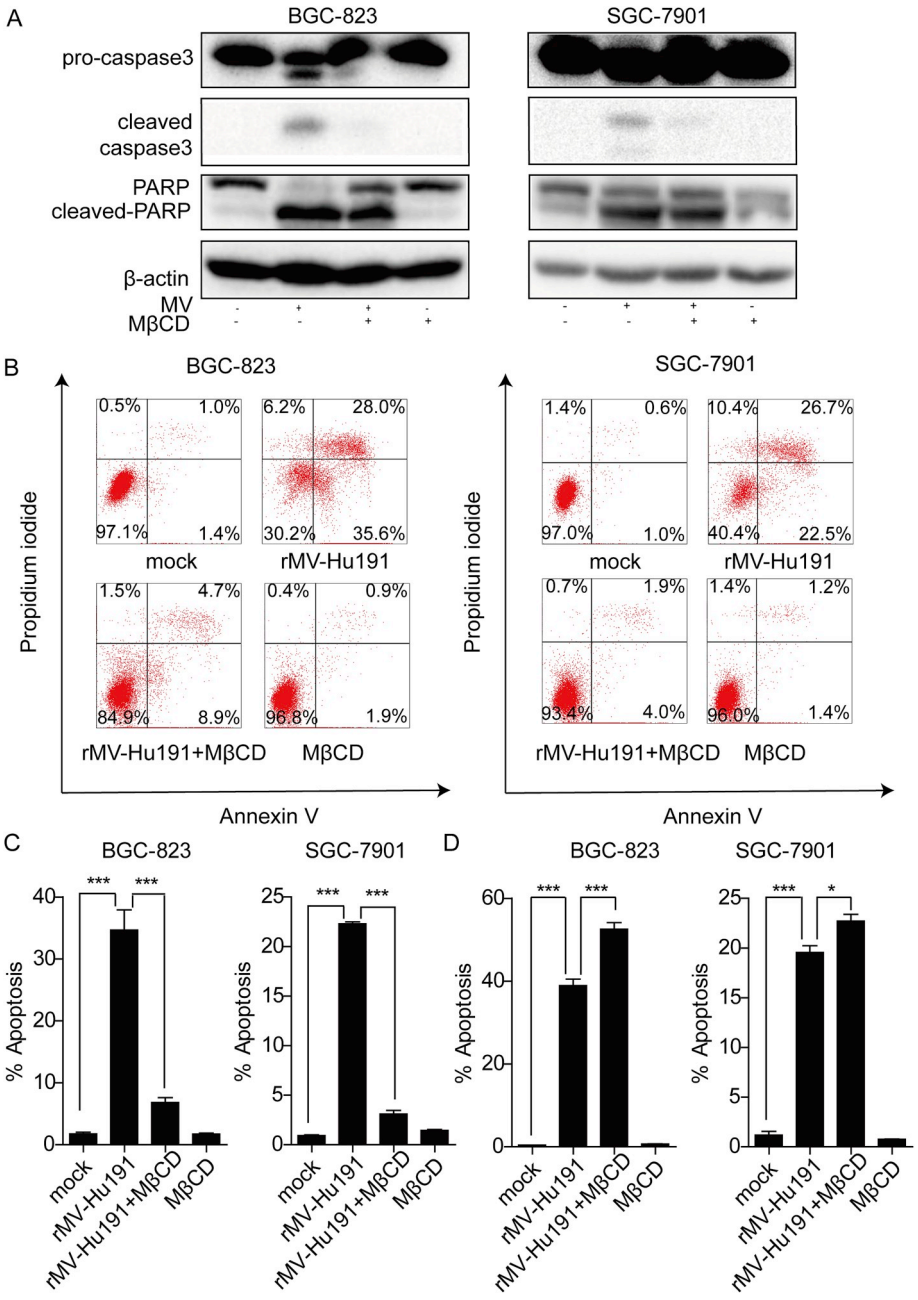

Fig. 4. The oncolytic effect of rMV-Hu191 required lipid raft integrity prior to infection. (A) Expression of apoptosis markers in BGC-823 and SGC-7901 cells infected by rMV-Hu191 (MOI = 1) for 48 h with or without MβCD treatment (5 mM, 2 h) prior to infection. (B–C) Cell apoptosis rate in BGC-823 and SGC-7901 cells infected by rMV-Hu191 for 48 h with or without MβCD treatment prior to infection. (D) MβCD (5 mM, 2 h) was added to cells after 2 h' infection by rMV-Hu191 (MOI = 1), cell apoptosis rate in GC cell lines 48 h after infection. *:P < 0.05, **:P < 0.01, ***:P < 0.001.

observed for color change under light microscope before DAB chromogen was added. Two slides incubated with PBS instead of the primary antibody were used as the negative control. Sectioned tumor tissues were stained by In situ Apoptosis Detection Kit (TUNEL, Takara, Japan) following the manufacturer's instructions to analyze the presence of apoptotic cells in vivo. Tissue slides were observed and photographed under light microscope with companion software (Leica, Germany). For immunofluorescence analysis of MV-P, sectioned tumor tissues were incubated with anti-MV-P antibody (ab43820, Abcam, UK) for 30 min at RT, followed by Alexa Fluor 594 conjugated donkey anti-mouse IgG (H + L) (#1608644, Life Technologies, USA), and then DAPI (Beyotime, China) in the dark. Slides were photographed using a Zeiss cLSM780 confocal laser scanning microscope and companion software.

2.10. Statistical analysis

Each experiment was repeated at least three times, with 3–5 parallel repeats, and data were presented as mean ± SE. Statistical significance between any two groups was analyzed by Student's *t*-test in GraphPad Prism software (v5.0, GraphPad Software, USA). Survival data was analyzed by the Kaplan-Meier method, and the log-rank test was used to test for significance between all the groups. P value of < 0.05 was considered statistically significant. P value of < 0.01 was considered highly significant.

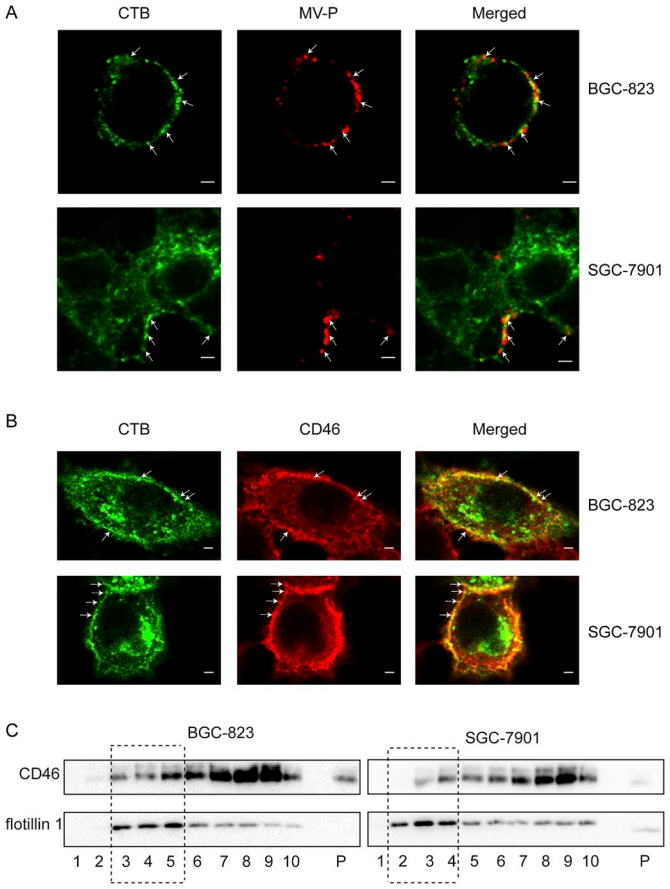

Fig. 5. Localization viral particle and CD46 in lipid raft microdomains. (A) Measles virus P protein (MV-P) is partly localized in lipid rafts domains labelled with cholera toxin B (CTB) 120 min after infection revealed by immunofluorescence in BGC-823 and SGC-7901 cells. Arrows indicate areas with colocalization of the two probes. Scale bar = 2 μm. (B) CD46 is partly localized in lipid rafts domains labelled with CTB 120 min after infection revealed by immunofluorescence in BGC-823 and SGC-7901 cells. Arrows indicate areas with colocalization of the two probes. Scale bar = 2 μm. (C) BGC-823 and SGC-7901 cells were solubilized by 0.5% TritonX-100 for 20 min on ice. The distribution of CD46 and lipid raft marker flotillin 1 in the sucrose gradient (fractions labelled 1 to 10 from top to bottom) and the insoluble pellet (P) is shown. Circled area indicates the location of lipid rafts in the density gradient.

2.11. Key resources table

Resource	Source	Identifier
Antibodies		
Alexa Fluor 594 conjugated donkey anti-mouse IgG		
anti-caspase-3		
anti-CD46		
anti-cleaved caspase 3		
anti–flotillin 1		
anti-goat IgG		
anti-measles virus phosphoprotein		
anti-mouse IgG		
anti-MV-P		
anti-nectin-4		
anti-PARP		
anti-ß-actin		
HRP-conjugated anti-rabbit IgG		
CellLine		
BGC-823		
SGC-7901		
Vero cells		
Chemical		
crystal violet		
DAPI		
fluorescein isothiocyanate		
hematoxylin		
methyl-ß-cyclodextrin		
penicillin-streptomycin		
phosphate buffered saline		
staurosporine		
STS		
Protein		
Alexa Fluor 594 conjugated cholera toxin subunit B	**N/A**	**N/A**
ProteinPeptide		
Annexin V		

3. Results

3.1. The oncolytic effect of rMV-Hu191 virus in human GC cells lines

After BGC-823 and SGC-7901 cells were incubated with rMV-Hu191, binding of virus onto the cells reached saturation within 2 h (Fig. S1A). Thus incubation time of rMV-Hu191 with GC cells was set at 2 h in the following experiments to allow viral binding. Furthermore, rMV-Hu191 replicated in both cell lines, reaching a peak titer at 48 h after infection in BGC-823 cells, and 72 h in SGC-7901 cells (Fig. S1B). At 24 h after infection, successful infection was also proved by presentation of virus particles in the cytosol visualized by MV-P protein (Fig. S1C), and oncolytic effect could be observed by formation of syncytia. For cell viability after viral infection (Fig. 1A–B), in both cell lines, reduction of viability was first observed within 48 h after infection, and the antitumor potency of rMV-Hu191 demonstrated dose and time dependent manners. Infection of rMV-Hu191 at MOIs of 0.1 and 1 elicited dramatic CPEs in dose and time dependent manners in both BGC-823 and SGC-7901 cells (Fig. 1C).

3.2. rMV-Hu191 induced caspase-dependent apoptosis in human GC cell lines

After BGC-823 and SGC-7901 cells were infected with rMV-Hu191 at a MOI of 0.5, the proportion of apoptotic cells was significantly increased in a time-dependent manner (Fig. 2A). In BGC-823 cells, the apoptotic rate after rMV-Hu191 infection was 3%, 23%, 28% and 43% at 24, 48, 72 and 96 h respectively; however, the apoptosis rate at the mock treated group was only 2%. In SGC-7901 cells, the apoptotic rate after rMV-Hu191 infection was 1%, 6%, 19% and 26% at 24, 48, 72 and 96 h respectively, while the rate was only 1% in mock treated group. To examine whether apoptosis induced by rMV-Hu191 was a caspase cascade, the expression of caspase 3 and PARP was examined (Fig. 2B, for repeated analysis of apoptotic markers by Western blotting, see Fig. S2). Upon infection with rMV-Hu191, the activation of caspase 3 and PARP, indicated by the expression of the cleaved forms, was significantly increased in time and dose-dependent manners. Moreover, co-treatment with Z-VAD for 72 h suppressed activation of caspase 3 and PARP in both cell lines (Fig. 2C). Densitometry analysis confirmed highly significant decrease of caspase 3 activation ($P < 0.01$), and significant decrease of PARP activation ($P < 0.05$) in both cell lines (Fig. 2D). Flow cytometry revealed that the increase in apoptosis was partially reversed in the presence of Z-VAD (Fig. 2E). In summary, it was shown that rMV-Hu191 induced caspase-dependent apoptosis in human GC cells.

3.3. Integrity of lipid rafts was required for rMV-Hu191 viral entry, but not for binding or replication

Validity of MβCD treatment to impair lipid raft integrity by dissolving cholesterol from the plasma membranes was verified by lack of flotillin 1 recovered in the buoyant density fractions after solubilization by non-ionic detergent (Fig. S4). After lipid rafts were disrupted by MβCD before viral infection, expression of MV-P in cell lysates was

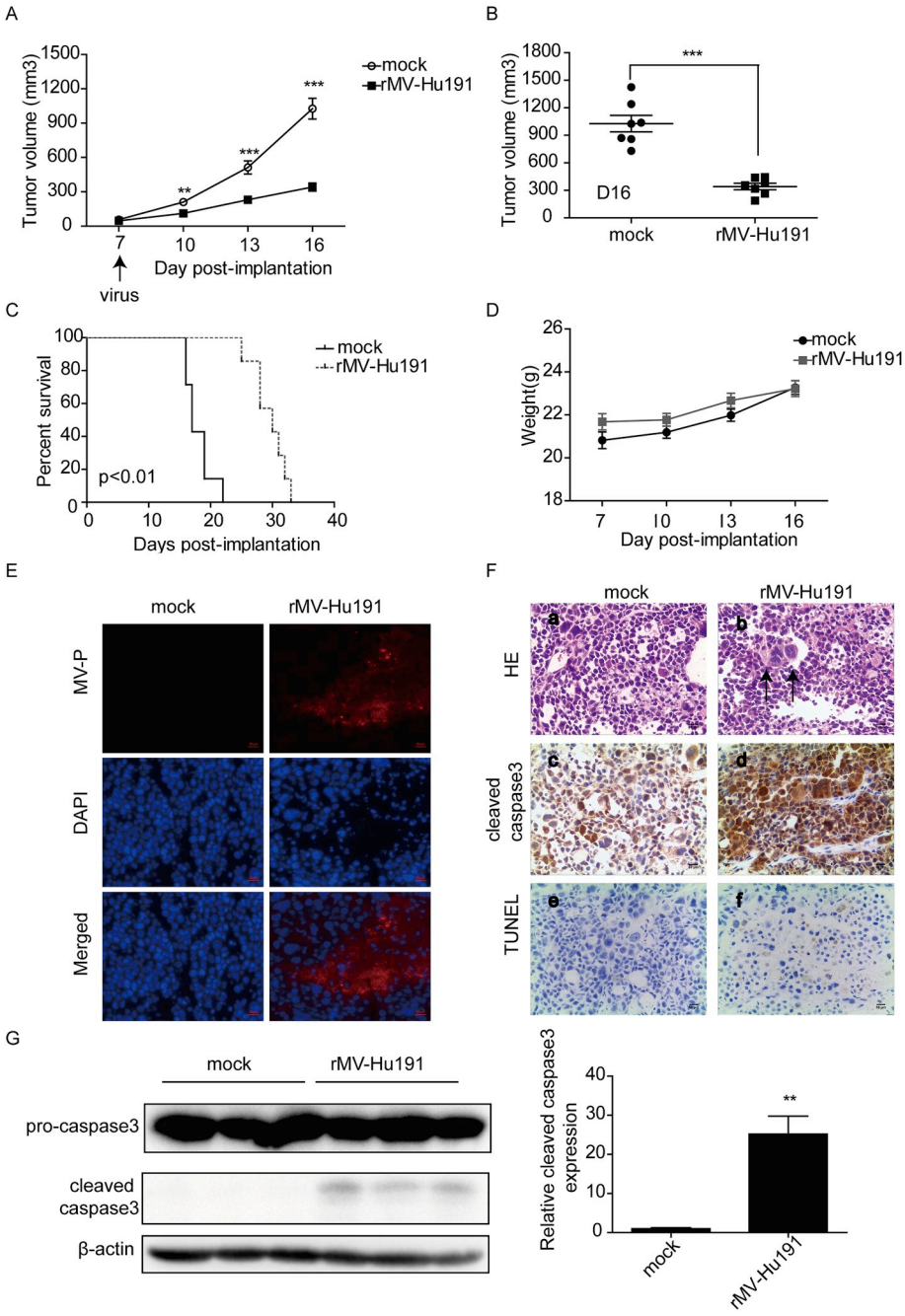

Fig. 6. The oncolytic effect of intratumoral rMV-Hu191 in GC tumor models established in nude mice. (A) Tumor growth in mice bearing GC xenografts with or without intratumoral rMV-Hu191 injections. (B) Difference in tumor volume on post-implantation day 16. (C) The Kaplan-Meier survival curves of mice from rMV-Hu191 and mock-treated groups. (D) Monitoring of body weights of mice in the two groups after tumor implantation. (E) Detection of MV by tissue immunofluorescence of MV-P protein. Scale bar = 20 μm. (F) Formation of syncytia (a–b), expression of cleaved caspase 3 (c–d), and presence of in situ apoptosis (e–f) in tumor tissues from rMV-Hu191 and mock treated mice. Arrows indicate syncytia. Scale bar = 50 μm. (F) Levels of cleaved caspase 3 expression from tumor tissues of the two groups, and the quantitative densitometry analysis. **:P < 0.01,***:P < 0.001.

decreased in both BGC-823 and SGC-7901 cells (Fig. 3A–B). Consistently, titers of viral particles were significantly reduced (Fig. 3C). However, from titration of the virus-containing culture medium after 2 h' incubation, the amount of unbound virus remained the same either with or without MβCD treatment (Fig. 3D). Consistently, the amount of MV-P recovered in the cell lysates did not vary with or without pre-treatment of MβCD (Fig. 3E–F). In Fig. 3G, cells were incubated with virus for 2 h, then cultured for another 4 h. MβCD was added at 6 h after infection to exercise possible effect on viral replication only. Viral titer was determined at 8, 12 and 24 h after infection. The above data showed there was no significant difference in viral titers detected at 24 h either with or without MβCD treatment when MβCD was added 6 h after infection.

3.4. rMV-Hu191-induced apoptosis was dependent on lipid raft integrity prior to viral binding

MβCD treatment was applied in GC cells either 2 h before incubation with rMV-Hu191, or after 2 h' incubation to allow viral binding. When lipid raft integrity was impaired by MβCD prior to viral infection, the expression of apoptotic marker proteins was decreased (Fig. 4A). Consistently, the ratio of apoptotic cells decreased from 35% to 7% in BGC-823, and from 22% to 3% in SGC-7901 cells when pre-treated with MβCD (Fig. 4B–C). On the other hand, if MβCD was administered after rMV-Hu191 incubation for 2 h, allowing sufficient time for viral binding, the ratio of apoptotic cells was not decreased by lipid raft disruption in both GC cell lines (Fig. 4D). In fact, the ratio of apoptotic cells was increased when lipid raft integrity was impaired after viral binding. Taken together, the data suggested that lipid raft integrity prior to viral binding was required for rMV-Hu191-induced apoptosis in

GC cells, while lipid raft disruption after viral binding did not impair apoptosis induction.

3.5. Viral particles and CD46 were both partially localized in lipid rafts

CTB conjugated to fluorescent probe was used to visualize lipid rafts. After 2 h' incubation, MV-P was found to be associated with CTB in part (Fig. 5A). CD46, a MV receptor expressed in both cell lines, was also found to be partially colocalized with CTB (Fig. 4B). More fluorescent images showing colocalization of MV-P and CD46 with CTB are shown in Fig. S3. Furthermore, lipid rafts were extracted from homogenized cell membrane preparations as detergent-resistant membranes and were identified by a common lipid raft marker, flotillin 1, which were mostly recovered in the buoyant density in the solubilized membrane preparations in both BGC-823 (fractions 3–5) and SGC-7901 (fractions 2–4) cells (Fig. 5C). Consistent with colocalization revealed by immunofluorescence, a small fraction of CD46 was recovered in the buoyant density fractions together with flotillin 1 (Fig. 5C). On the other hand, nectin-4, another membrane MV receptor expressed in GC cell lines, was not recovered in fractions containing detergent-resistant membranes (Fig. S5).

IF images also revealed the distribution patterns of MV-P at different time points of viral infection. In Fig. 3A, at 120 min of viral incubation, most MV-P were located on the cell surface. However, at 24 h (Fig. S1C), most MV-P were observed in the cytosol.

3.6. Intratumoral administration of rMV-Hu191 induced tumor regression and apoptosis in GC xenografts

Human GC xenografts were successfully established in nude mice. The in vivo tumor-suppressive effect of rMV-Hu191 was first detected on days 10 after tumor implantation, which was 3 days after treatment (Fig. 6A). The therapeutic efficacy increased over time, resulting in effective suppression of tumor growth from post-implantation day 10 to day 16 (Fig. 6A), and most significantly on day 16 after 6 injections (Fig. 6B). rMV-Hu191 treatment resulted in a significant increase in the survival rate (Fig. 6C). The median survival of rMV-Hu191 treated group was 30 days, as compared with 17 days in the mock treated group. The median survival of rMV-Hu191-treated animals, with a 1.76-fold increase, was significantly longer than that of the mock treated group ($P < 0.01$) (Fig. 6C). Moreover, no significant difference in body weight between the two groups was observed (Fig. 6D). MV-P protein was detected in the tumor sections treated with rMV-Hu191, but not in the mock treated group (Fig. 6E). The CPE manifested by formation of syncytia was detected only in rMV-Hu191-treated tumors (Fig. 6F, ab). Thus rMV-Hu191 inhibited tumor growth and increased survival in mice with SGC-7901 GC xenografts. Furthermore, induction of apoptosis in tumor tissues was confirmed by analysis of both cleaved caspase 3 expression (Fig. 6F, cd) and in situ apoptosis (Fig. 6F, ef). Increase of cleaved caspase 3 expression was also confirmed in protein extracts from tumor tissues and quantitative analysis (Fig. 6G).

4. Discussion

There is a wide variety of oncolytic virus strains under clinical trials, including MV, HSV, adenovirus, and poliovirus, etc [41]. The MV Edmonston B vaccine strain is one the most intensively investigated drug candidate. MV vaccines have the advantage of being replicative and disseminating in the tumor tissues to achieve enhanced therapeutic effects [6,42]. With the same advantage, the Chinese Hu191 strain derivatives have been proved to be highly safe in the application of vaccination in China. Our study is the first to show that MV strains could serve as an oncolytic virotherapy candidate for GC.

From our data, the amount of rMV-Hu191 bound onto the cells reached saturation level after 2 h. Viral replication and oncolytic effect could be observed by measuring viral titer and by formation of syncytia from 24 h after infection, peaked at 48 h after infection, then subdued perhaps due to decrease of viable cells. Consistently, by IF imaging, the majority of MV particles was found on the cell surface after 2 h' incubation. However, after 24 h, most viral particles were present in the cytosol. All suggesting viral binding mostly occurred in the first 2 h, viral entry and replication happened afterwards. The two human GC cell lines were both susceptible to the cytotoxic effect of rMV-Hu191, but to different extent. The virus eliminated the BGC-823 cells more readily, whereas its cytotoxic effect on SGC-7901 cells was exhibited at later time. The characteristics of each cell line that render differences in susceptibility are yet to be discovered by molecular profiling.

From our data, rMV-Hu191 viral particles most bound to cell surface after 2 h' incubation with colocalization with lipid raft marker CTB, and were mostly present in the cytosol after 24 h. TCID 50 curves also indicate that most viral replication took place between 6 and 24 h after initial infection. Lipid raft integrity prior to viral binding was required for the subsequent production of rMV-Hu191 viral particles, as well as induction of apoptosis. After disruption of lipid rafts, the amount of viral particles bound to cells was not decreased, however, decrease in the amount of virus produced in the cells exhibited after 24 h. By dissolving lipid rafts between 6 and 24 h after initial viral infection, when viral entry had occurred and the viruses were undergoing replication, it was found that lack of lipid raft integrity did not affect actual viral replication, thus lipid raft is only important at early stage of viral entry. In other experiments, we also found that rMV-Hu191 infectivity in BGC-823 and SGC-7901 cells was inhibited after treatment by chloroquine, a drug that disrupts the endocytic pathway by increasing the normally acid pH in subcellular organelles including endosomes and lysosomes (Fig. S6). Such discovery is consistent with literature reports suggesting lipid rafts could serve as the platform for virus endocytosis [28]. Intracellular assembly of MV may also require lipid rafts [32], however, our data suggested otherwise since viral replication did not require lipid raft integrity.

In vivo studies confirmed that intratumoral rMV-Hu191 injection resulted in a significant reduction in tumor growth, as well as dramatic enhancement in survival time in mice bearing human SGC-7901 xenografts. No significant toxicity resulting in difference in body weight was observed between the mock treated group and rMV-Hu191 treated group. It is known that MV does not grow well in mice due to lack of expression of viral receptors [43]. Side effect induced by rMV-Hu191 should be evaluated in transgenic mice or squirrel monkeys by future studies.

Apoptosis is a form of programmed cell death orchestrated by activation of caspases and can occur either via mitochondria-mediated pathway (intrinsic signaling) or via the ligation of the cell death receptor (extrinsic signaling) [44,45]. The MV vaccine strain Edmonston B could induce apoptosis [46]. In this study, we found that rMV-Hu191 exhibited significant antitumor effect against GC through induction of caspase-dependent apoptosis both in vitro and vivo. In rMV-Hu191 infected GC cells, ratio of apoptotic cells was increased, and activation of caspase 3 and PARP was identified in time and dose dependent manners. Furthermore, the pan-caspase inhibitor Z-VAD could partially reverse the induction of apoptotic cell death after rMV-Hu191 infection. In SGC-7901 xenografts, induction of caspase-dependent apoptosis was approved by in situ caspase 3 immuno-detection and TUNEL assay. Same as many other oncolytic virus strains, the capability to induce caspase-dependent apoptosis seems to be the major mechanism for rMV-Hu191 to inhibit GC.

Our data suggested that CD46 was localized in the lipid rafts in a small fraction. In literature reports, whether CD46 is recruited to the lipid raft domains lack consistency, and seems to be determined by the nature of the experimental model [29,31,47]. It was reported that expression of CD46 could be down-regulated following persistent MV infection [48]. We have also found that the amount of CD46 associated with lipid rafts was decreased after rMV-Hu191 infection (data not shown). CD46 might be recruited to the lipid rafts and endocytosed in

order to facilitate MV viral entry. It should be noted that nectin-4, the other MV receptor on GC cells, was not localized in lipid rafts, thus viral entry through lipid raft-independent mechanism could not be excluded. A lot more details needs to be clarified before the mechanism of rMV-Hu191 viral entry can be revealed completely.

In conclusion, our findings suggested that recombinant Chinese Hu191 MV vaccine strain has potent therapeutic efficacy against human GC both in vivo and in vitro. rMV-Hu191-induced apoptosis in GC cells is dependent on caspase activation, and requires lipid raft integrity. Lipid rafts serve as a platform to facilitate entry of rMV-Hu191 into the GC cells at least in part, and CD46 could be involved. The characterization of the underlying mechanism may provide a theoretical basis for utilizing this attenuated virus as a novel oncolytic agent against human GC.

Conflicts of interest

The authors declared that they have no conflicts of interest to this work.

We declare that we do not have any commercial or associative interest that represents a conflict of interest in connection with the work submitted.

Authors' contributions

Conceived and designed the experiments: Zhengyan Zhao, Xi Chen, Yao Lv. Performed the experiments: Yao Lv, Duo-Zhou, Dong-ming Zhou, Wei-zhong Gu, Chu-di Zhang, Rong-xian Liu. Wrote the manuscript: Yao Lv, Zhengyan Zhao, Xi Chen.

Acknowledgements

This work was supported partly by the Zhejiang Provincial Science technology research program (2017C33047).The authors thank MD Deng-ming Lai from Children's Hospital, Zhejiang University School of Medicine, Hangzhou for his technical assistance.

Abbreviations

MV	measles virus
GC	gastric cancer
rMV-Hu191	recombinant Chinese Hu191
MβCD	methyl-β-cyclodextrin
SFDA	state food and drug administration
MV-F	measles virus fusion protein
MV-H	measles virus haemagglutinin
MV-P	measles virus phosphoprotein
MV-N	measles virus nucleoprotein
MV-M	measles virus matrix protein
MV-L	measles virus RNA polymerase
MV-V and MV-C	measles virus two non-structural proteins
SLAM	signaling lymphocyte-activation molecule
CD150	cluster of differentiation 150
CD46	cluster of differentiation 46
ATCC	American Type Culture Collection
DMEM	Dulbecco's modified Eagle's medium
TCID 50	tissue culture infective dose
PBS	phosphate buffered saline
MOI	multiplicity of infection
STS	staurosporine
Z-VAD	Z-VAD-FMK
CCK-8	Cell Counting Kit-8
PFA	paraformaldehyde
RT	room temperature
IF	immunofluorescence
CPEs	cytopathic effects
HE	hematoxylineosin
PARP	poly-ADP-ribose polymerase
FITC	fluorescein isothiocyanate
PI	propidium iodide
CTB	cholera toxin subunit B
CQ	chloroquine

Appendix A. Supplementary data

Supplementary data to this article can be found online at https://doi.org/10.1016/j.canlet.2019.06.010.

References

[1] M. Liang, Oncorine, the world first oncolytic virus medicine and its update in China, Curr. Cancer Drug Targets 18 (2018) 171–176.
[2] P. Alberts, E. Olmane, L. Brokane, Z. Krastina, M. Romanovska, K. Kupcs, S. Isajevs, G. Proboka, R. Erdmanis, J. Nazarovs, D. Venskus, Long-term treatment with the oncolytic ECHO-7 virus Rigvir of a melanoma stage IV M1c patient, a small cell lung cancer stage IIIA patient, and a histiocytic sarcoma stage IV patient-three case reports, APMIS : APMIS (Acta Pathol. Microbiol. Immunol. Scand.) 124 (2016) 896–904.
[3] R.H. Andtbacka, H.L. Kaufman, F. Collichio, T. Amatruda, N. Senzer, J. Chesney, K.A. Delman, L.E. Spitler, I. Puzanov, S.S. Agarwala, M. Milhem, L. Cranmer, B. Curti, K. Lewis, M. Ross, T. Guthrie, G.P. Linette, G.A. Daniels, K. Harrington, M.R. Middleton, W.H. Miller Jr., J.S. Zager, Y. Ye, B. Yao, A. Li, S. Doleman, A. VanderWalde, J. Gansert, R.S. Coffin, Talimogene Laherparepvec improves durable response rate in patients with advanced melanoma, J. Clin. Oncol. : official journal of the American Society of Clinical Oncology 33 (2015) 2780–2788.
[4] J.B. Guillerme, M. Gregoire, F. Tangy, J.F. Fonteneau, Antitumor virotherapy by attenuated measles virus (MV), Biology 2 (2013) 587–602.
[5] L. Russell, K.W. Peng, The emerging role of oncolytic virus therapy against cancer, Chin. Clin. Oncol. 7 (2018) 16.
[6] A. Dispenzieri, C. Tong, B. LaPlant, M.Q. Lacy, K. Laumann, D. Dingli, Y. Zhou, M.J. Federspiel, M.A. Gertz, S. Hayman, F. Buadi, M. O'Connor, V.J. Lowe, K.W. Peng, S.J. Russell, Phase I trial of systemic administration of Edmonston strain of measles virus genetically engineered to express the sodium iodide symporter in patients with recurrent or refractory multiple myeloma, Leukemia 31 (2017) 2791–2798.
[7] P.C. Jordan, C. Liu, P. Raynaud, M.K. Lo, C.F. Spiropoulou, J.A. Symons, L. Beigelman, J. Deval, Initiation, extension, and termination of RNA synthesis by a paramyxovirus polymerase, PLoS Pathog. 14 (2018) e1006889.
[8] G.F. Rall, Measles virus 1998-2002: progress and controversy, Annu. Rev. Microbiol. 57 (2003) 343–367.
[9] Y. Zhang, J. Zhou, W.J. Bellini, W. Xu, P.A. Rota, Genetic characterization of Chinese measles vaccines by analysis of complete genomic sequences, J. Med. Virol. 81 (2009) 1477–1483.
[10] D. Zhao, P. Chen, H. Yang, Y. Wu, X. Zeng, Y. Zhao, Y. Wen, X. Zhao, X. Liu, Y. Wei, Y. Li, Live attenuated measles virus vaccine induces apoptosis and promotes tumor regression in lung cancer, Oncol. Rep. 29 (2013) 199–204.
[11] Y. Wang, R. Liu, M. Lu, Y. Yang, D. Zhou, X. Hao, D. Zhou, B. Wang, J. Li, Y.W. Huang, Z. Zhao, Enhancement of safety and immunogenicity of the Chinese Hu191 measles virus vaccine by alteration of the S-adenosylmethionine (SAM) binding site in the large polymerase protein, Virology 518 (2018) 210–220.
[12] R.L. Siegel, K.D. Miller, A. Jemal, Cancer statistics, CA A Cancer J. Clin. 66 (2016) 7–30 2016.
[13] Z. Song, Y. Wu, J. Yang, D. Yang, X. Fang, Progress in the treatment of advanced gastric cancer, Tumour Biol 39 (2017) 1010428317714626.
[14] D. Zhou, W. Liu, S. Liang, B. Sun, A. Liu, Z. Cui, X. Han, L. Yuan, Apoptin-derived peptide reverses cisplatin resistance in gastric cancer through the PI3K-AKT signaling pathway, Cancer Med 7 (2018) 1369–1383.
[15] M.A. Lyes, S. Payne, P. Ferrell, S.V. Pizzo, S.T. Hollenbeck, R.E. Bachelder, Adipose stem cell crosstalk with chemo-residual breast cancer cells: implications for tumor recurrence, Breast Canc. Res. Treat. 174 (2) (2018) 413–422.
[16] T. Tsuji, M. Nakamori, M. Iwahashi, M. Nakamura, T. Ojima, T. Iida, M. Katsuda, K. Hayata, Y. Ino, T. Todo, H. Yamaue, An armed oncolytic herpes simplex virus expressing thrombospondin-1 has an enhanced in vivo antitumor effect against human gastric cancer, Int. J. Cancer 132 (2013) 485–494.
[17] W. Zhou, S. Dai, H. Zhu, Z. Song, Y. Cai, J.B. Lee, Z. Li, X. Hu, B. Fang, C. He, X. Huang, Telomerase-specific oncolytic adenovirus expressing TRAIL suppresses peritoneal dissemination of gastric cancer, Gene Ther. 24 (2017) 199–207.
[18] E.S. Haley, G.G. Au, B.R. Carlton, R.D. Barry, D.R. Shafren, Regional administration of oncolytic Echovirus 1 as a novel therapy for the peritoneal dissemination of gastric cancer, J. Mol. Med. (Berl.) 87 (2009) 385–399.
[19] X. Bu, M. Li, Y. Zhao, S. Liu, M. Wang, J. Ge, Z. Bu, Y. Yan, Genetically engineered Newcastle disease virus expressing human interferon-lambda1 induces apoptosis in gastric adenocarcinoma cells and modulates the Th1/Th2 immune response, Oncol. Rep. 36 (2016) 1393–1402.
[20] R. Yokoda, B.M. Nagalo, M. Arora, J.B. Egan, J.M. Bogenberger, T.T. DeLeon, Y. Zhou, D.H. Ahn, M.J. Borad, Oncolytic virotherapy in upper gastrointestinal tract cancers, Oncolytic Virotherapy 7 (2017) 13–24.

[21] F. Xu, S. Tanaka, H. Watanabe, Y. Shimane, M. Iwasawa, K. Ohishi, T. Maruyama, Computational analysis of the interaction energies between amino acid residues of the measles virus hemagglutinin and its receptors, Viruses (2018) 10.
[22] B. Wang, J. Liu, L. Na Ma, H. Xiao, Y. Wan, Y. Li, Z. Wang, L. Fan, C. Lan, M. Yang, L. Hu, Y. Wei, X. Bian, D. Chen, J. Wang, Chimeric 5/35 adenovirus-mediated Dickkopf-1 overexpression suppressed tumorigenicity of CD44+ gastric cancer cells via attenuating Wnt signaling, J. Gastroenterol. 48 (2013) 798–808.
[23] Y. Zhang, J. Zhang, Q. Shen, W. Yin, H. Huang, Y. Liu, Q. Ni, High expression of Nectin-4 is associated with unfavorable prognosis in gastric cancer, Oncol Lett 15 (2018) 8789–8795.
[24] K. Simons, E. Ikonen, Functional rafts in cell membranes, Nature 387 (1997) 569–572.
[25] S. Staubach, F.G. Hanisch, Lipid rafts: signaling and sorting platforms of cells and their roles in cancer, Expert Rev. Proteomics 8 (2011) 263–277.
[26] H. Tang, Y. Mori, Human herpesvirus-6 entry into host cells, Future Microbiol. 5 (2010) 1015–1023.
[27] B. Bhattacharya, P. Roy, Role of lipids on entry and exit of bluetongue virus, a complex non-enveloped virus, Viruses 2 (2010) 1218–1235.
[28] D.K. Verma, D. Gupta, S.K. Lal, Host lipid rafts play a major role in binding and endocytosis of influenza a virus, Viruses 10 (2018) 650.
[29] M.J. Ludford-Menting, B. Crimeen-Irwin, J. Oliaro, A. Pasam, D. Williamson, N. Pedersen, P. Guillaumot, D. Christansen, S. Manie, K. Gaus, S.M. Russell, The reorientation of T-cell polarity and inhibition of immunological synapse formation by CD46 involves its recruitment to lipid rafts, J Lipids 2011 (2011) 521863.
[30] A. Ghannam, D. Hammache, C. Matias, M. Louwagie, J. Garin, D. Gerlier, High-density rafts preferentially host the complement activator measles virus F glycoprotein but not the regulators of complement activation, Mol. Immunol. 45 (2008) 3036–3044.
[31] S. Serge n manié, S. Vincent, D. gerlier, Measles virus structural components are enriched into lipid raft microdomains: a potential cellular location for virus assembly, J. Virol. 74 (2000) 305–311.
[32] S. Vincent, D. Gerlier, S.N. Manie, Measles virus assembly within membrane rafts, J. Virol. 74 (2000) 9911–9915.
[33] S.C. Lim, H.Q. Duong, J.E. Choi, T.B. Lee, J.H. Kang, S.H. Oh, S.I. Han, Lipid raft-dependent death receptor 5 (DR5) expression and activation are critical for ursodeoxycholic acid-induced apoptosis in gastric cancer cells, Carcinogenesis 32 (2011) 723–731.
[34] L. Xu, X. Qu, X. Hu, Z. Zhu, C. Li, E. Li, Y. Ma, N. Song, Y. Liu, Lipid raft-regulated IGF-1R activation antagonizes TRAIL-induced apoptosis in gastric cancer cells, FEBS Lett. 587 (2013) 3815–3823.
[35] M.A. Ramakrishnan, Determination of 50% endpoint titer using a simple formula, World J. Virol. 5 (2016) 85–86.
[36] P. Nagy, Lipid rafts and the local density of ErbB proteins influence the biological role of homo- and heteroassociations of ErbB2, J. Cell Sci. 115 (2002) 4251–4262.
[37] I. Levental, S. Veatch, The continuing mystery of lipid rafts, J. Mol. Biol. 428 (2016) 4749–4764.
[38] A.I. Nagasato, H. Yamashita, M. Matsuo, K. Ueda, N. Kioka, The distribution of vinculin to lipid rafts plays an important role in sensing stiffness of extracellular matrix, Biosci. Biotechnol. Biochem. 81 (2017) 1136–1147.
[39] X. Chen, A. Jen, A. Warley, M.J. Lawrence, P.J. Quinn, R.J. Morris, Isolation at physiological temperature of detergent-resistant membranes with properties expected of lipid rafts: the influence of buffer composition, Biochem. J. 417 (2009) 525–533.
[40] P.E. Bickel, P.E. Scherer, J.E. Schnitzer, P. Oh, M.P. Lisanti, H.F. Lodish, Flotillin and epidermal surface antigen define a new family of caveolae-associated integral membrane proteins, J. Biol. Chem. 272 (1997) 13793–13802.
[41] S.G. Warner, M.P. O'Leary, Y. Fong, Therapeutic oncolytic viruses: clinical advances and future directions, Curr. Opin. Oncol. 29 (2017) 359–365.
[42] S.C. Zhang, W.L. Wang, W.S. Cai, K.L. Jiang, Z.W. Yuan, Engineered measles virus Edmonston strain used as a novel oncolytic viral system against human hepatoblastoma, BMC Canc. 12 (2012) 427.
[43] S. Lal, D. Carrera, J.J. Phillips, W.A. Weiss, C. Raffel, An oncolytic measles virus-sensitive Group 3 medulloblastoma model in immune-competent mice, Neuro Oncol. 20 (2018) 1606–1615.
[44] L. Galluzzi, I. Vitale, S.A. Aaronson, J.M. Abrams, D. Adam, P. Agostinis, E.S. Alnemri, L. Altucci, I. Amelio, D.W. Andrews, M. Annicchiarico-Petruzzelli, A.V. Antonov, E. Arama, E.H. Baehrecke, N.A. Barlev, N.G. Bazan, F. Bernassola, M.J.M. Bertrand, K. Bianchi, M.V. Blagosklonny, K. Blomgren, C. Borner, P. Boya, C. Brenner, M. Campanella, E. Candi, D. Carmona-Gutierrez, F. Cecconi, F.K. Chan, N.S. Chandel, E.H. Cheng, J.E. Chipuk, J.A. Cidlowski, A. Ciechanover, G.M. Cohen, M. Conrad, J.R. Cubillos-Ruiz, P.E. Czabotar, V. D'Angiolella, T.M. Dawson, V.L. Dawson, V. De Laurenzi, R. De Maria, K.M. Debatin, R.J. DeBerardinis, M. Deshmukh, N. Di Daniele, F. Di Virgilio, V.M. Dixit, S.J. Dixon, C.S. Duckett, B.D. Dynlacht, W.S. El-Deiry, J.W. Elrod, G.M. Fimia, S. Fulda, A.J. Garcia-Saez, A.D. Garg, C. Garrido, E. Gavathiotis, P. Golstein, E. Gottlieb, D.R. Green, L.A. Greene, H. Gronemeyer, A. Gross, G. Hajnoczky, J.M. Hardwick, I.S. Harris, M.O. Hengartner, C. Hetz, H. Ichijo, M. Jaattela, B. Joseph, P.J. Jost, P.P. Juin, W.J. Kaiser, M. Karin, T. Kaufmann, O. Kepp, A. Kimchi, R.N. Kitsis, D.J. Klionsky, R.A. Knight, S. Kumar, S.W. Lee, J.J. Lemasters, B. Levine, A. Linkermann, S.A. Lipton, R.A. Lockshin, C. Lopez-Otin, S.W. Lowe, T. Luedde, E. Lugli, M. MacFarlane, F. Madeo, M. Malewicz, W. Malorni, G. Manic, J.C. Marine, S.J. Martin, J.C. Martinou, J.P. Medema, P. Mehlen, P. Meier, S. Melino, E.A. Miao, J.D. Molkentin, U.M. Moll, C. Munoz-Pinedo, S. Nagata, G. Nunez, A. Oberst, M. Oren, M. Overholtzer, M. Pagano, T. Panaretakis, M. Pasparakis, J.M. Penninger, D.M. Pereira, S. Pervaiz, M.E. Peter, M. Piacentini, P. Pinton, J.H.M. Prehn, H. Puthalakath, G.A. Rabinovich, M. Rehm, R. Rizzuto, C.M.P. Rodrigues, D.C. Rubinsztein, T. Rudel, K.M. Ryan, E. Sayan, L. Scorrano, F. Shao, Y. Shi, J. Silke, H.U. Simon, A. Sistigu, B.R. Stockwell, A. Strasser, G. Szabadkai, S.W.G. Tait, D. Tang, N. Tavernarakis, A. Thorburn, Y. Tsujimoto, B. Turk, T. Vanden Berghe, P. Vandenabeele, M.G. Vander Heiden, A. Villunger, H.W. Virgin, K.H. Vousden, D. Vucic, E.F. Wagner, H. Walczak, D. Wallach, Y. Wang, J.A. Wells, W. Wood, J. Yuan, Z. Zakeri, B. Zhivotovsky, L. Zitvogel, G. Melino, G. Kroemer, Molecular mechanisms of cell death: recommendations of the nomenclature committee on cell death 2018, Cell Death Differ. 25 (2018) 486–541.
[45] C. Rogers, T. Fernandes-Alnemri, L. Mayes, D. Alnemri, G. Cingolani, E.S. Alnemri, Cleavage of DFNA5 by caspase-3 during apoptosis mediates progression to secondary necrotic/pyroptotic cell death, Nat. Commun. 8 (2017) 14128.
[46] A. Chen, Y. Zhang, G. Meng, D. Jiang, H. Zhang, M. Zheng, M. Xia, A. Jiang, J. Wu, C. Beltinger, J. Wei, Oncolytic measles virus enhances antitumour responses of adoptive CD8(+)NKG2D(+) cells in hepatocellular carcinoma treatment, Sci. Rep. 7 (2017) 5170.
[47] H. Tang, A. Kawabata, M. Takemoto, K. Yamanishi, Y. Mori, Human herpesvirus-6 infection induces the reorganization of membrane microdomains in target cells, which are required for virus entry, Virology 378 (2008) 265–271.
[48] S.Y. Akiko Hirano, Kazunori Iwata, Jennifer Korte-sarfaty, S.N. Tsukasa Seya, Timothy C. Wong, Human cell receptor CD46 is down regulated through recognitionof a membrane-proximal region of the cytoplasmic domain in persistent measles virus infection, J. Virol. 70 (1996) 6929–6936.